Journal of the American College of Cardiology
© 2006 by the American College of Cardiology Foundation
Published by Elsevier Inc.

Vol. 48, No. 10, 2006
ISSN 0735-1097/06/$32.00
doi:10.1016/j.jacc.2006.08.030

Left Ventricular Structure and Function

Basic Science for Cardiac Imaging

Partho P. Sengupta, MBBS, MD, DM,* Josef Korinek, MD,*
Marek Belohlavek, MD, PHD, FACC, FESC,* Jagat Narula, MBBS, MD, DM, PHD, FACC, FAHA,†
Mani A. Vannan, MBBS, FACC,† Arshad Jahangir, MD, FACC,*
Bijoy K. Khandheria, MD, FESC, FASE, FACC‡
Rochester, Minnesota; Irvine, California; and Scottsdale, Arizona

The myofiber geometry of the left ventricle (LV) changes gradually from a right-handed helix in the subendocardium to a left-handed helix in the subepicardium. In this review, we associate the LV myofiber architecture with emerging concepts of the electromechanical sequence in a beating heart. We discuss: 1) the morphogenesis and anatomical arrangement of muscle fibers in the adult LV; 2) the sequence of depolarization and repolarization; 3) the physiological inhomogeneity of transmural myocardial mechanics and the apex-to-base sequence of longitudinal and circumferential deformation; 4) the sequence of LV rotation; and 5) the link between LV deformation and the intracavitary flow direction observed during each phase of the cardiac cycle. Integrating the LV structure with electrical activation and motion sequences observed in vivo provides an understanding about the spatiotemporal sequence of regional myocardial performance that is essential for noninvasive cardiac imaging. (J Am Coll Cardiol 2006;48:1988–2001) © 2006 by the American College of Cardiology Foundation

Heart failure is a growing problem worldwide (1). Almost 5 million Americans have heart failure, and a further 550,000 are diagnosed with heart failure annually (2). The current biological models used for understanding the syndrome of heart failure are insufficient in explaining the benefits of several newer emerging therapies (3). These limitations may result from inaccuracies in modeling the structure and physiology of the left ventricle (LV), which becomes maladaptive and disorganized. A report from a recent National Institutes of Health meeting drew attention to the existing gaps in the understanding of the normal structure and function of a beating heart (4). In particular, the regional inhomogeneity of mechanical shortening and lengthening sequences in the LV wall, which result in a highly efficient global function of the normal heart, despite presence of structural anisotropy, remain contentious and incompletely characterized (5–8).

Normal ventricular function requires coordinated electrical activation and contraction. Given the 3-dimensional pattern of ventricular activation and contraction, the assessment of mechanical activation using conventional imaging methods is a complex task. Although electrical depolarization follows an anatomically predefined sequence in healthy individuals, physiological mechanical activity is characterized by a higher degree of nonuniformity (9). The impact of cardiac resynchronization therapy on global systolic and diastolic performance in dyssynchronous hearts particularly has renewed an interest in understanding the physiological nonuniformities of regional LV performance (10,11). Because QRS duration alone fails to predict reverse remodeling, imaging techniques with high temporal resolution have been actively sought for more accurate characterization of regional LV deformation (10,11). Simultaneous integration of LV muscle fiber geometry and function at a regional level with global sequence of cardiac deformation in different phases of the cardiac cycle remains an area of intense investigation.

In this review, we first summarize the parameters that are required for describing LV geometry and deformation. Further, we describe the emerging concepts regarding the sequence of electromechanical activation and LV intracavitary flow within the anatomical context of the helical myofiber arrangement of the LV wall.

LEFT VENTRICULAR GEOMETRY

Normal LV geometry has been conceptualized as a prolate ellipsoid shape (12) with its long-axis directed from apex to base. Therefore, short-axis cross sections of the LV should reveal a circular geometry. However, because of a curved posterolateral wall and a flat anterior wall (13), the short-axis cross sections obtained by

From the *Division of Cardiovascular Diseases, Mayo Clinic, Rochester, Minnesota; †Division of Cardiology, University of California at Irvine, Irvine, California; and the ‡Division of Cardiovascular Diseases, Mayo Clinic, Scottsdale, Arizona. This work was supported by grant HL68573 and, in parts, grants HL68555 and HL70363 from the National Institutes of Health and a Grant-in-Aid from the American Society of Echocardiography.

Manuscript received June 1, 2006; revised manuscript received August 29, 2006, accepted August 30, 2006.

Abbreviations and Acronyms

IVC = isovolumic contraction
IVR = isovolumic relaxation
LV = left ventricle/ventricular
MRI = magnetic resonance imaging

cardiac imaging techniques do not appear circular. In addition, the endocardial surface is extremely irregular because of the presence of papillary muscles and trabeculae (12). Significant nonuniformities also exist in the LV wall, particularly with regard to the thickness. The posterolateral wall is significantly thicker than the septum. A gradual thinning of the LV wall is observed toward the apical segments (13).

QUANTITATIVE TERMS IN LV MECHANICS

During a cardiac cycle, the LV wall shortens, thickens, and twists along the long axis. Shortening and thickening can be quantified by measuring regional strain. Strain or myocardial deformation from developing forces is expressed as either the fractional or the percent change from the original dimension (14). Positive radial strains represent wall thickening (radial deformation), whereas negative strains represent segment shortening (e.g., circumferential shortening, longitudinal shortening, and fiber shortening). These strains can be expressed either in a local cardiac coordinate system or a local fiber coordinate system (13). Three perpendicular axes orienting the global geometry of the LV define the local cardiac coordinate system: radial, circumferential, and longitudinal. The local fiber coordinate system is defined by the following: 1) the radial axis similar to the local cardiac coordinate system, 2) the fiber axis tangent to the surface and parallel to the local fiber orientation, and 3) the cross-fiber axis, tangent to the surface and perpendicular to the fiber.

Echocardiographic techniques like tissue Doppler imaging have excellent temporal resolution (<4 ms) and provide the instantaneous velocity of myocardial motion. The velocity data can be postprocessed for calculating parameters such as displacement, strain rate, and strain. Numerical integration of velocity over time results in displacement curves. Strain rate, which is the rate of change of deformation, is derived as a spatial derivative of velocity, whereas temporal integration of strain rate is used for calculating regional strain (14).

Left ventricular rotation, twist, and torsion are terms often used interchangeably in published reports for explaining the wringing motion of the LV. For this review, the term "rotation" will refer to the rotation of a short-axis sections of LV as viewed from the apical end and defined as the angle between radial lines connecting the center of mass of that specific cross-sectional plain to a specific point in the myocardial wall at end diastole and at any other time during systole (15). The unit of rotation is degrees or radians. The base and apex of the LV rotate in opposite directions. Twist defines the base to apex gradient in the rotation angle along the longitudinal axis of the LV and is expressed in degrees per centimeter or radians per meter (16). Torsion and twist are equivalent terms. Torsion also can be expressed as the axial gradient in the rotation angle multiplied by the average of the outer radii in apical and basal cross-sectional planes, thereby representing the shear deformation angle on the epicardial surface (unit degrees or radians) (17). This normalization can be used as a method for comparing torsion for different sizes of LV. When the apex-to-base difference in LV rotation is not normalized, the absolute difference (also in degrees or radians) is stated as the net LV twist angle (16).

DEVELOPMENTAL CHANGES

The heart increases in size by 2 orders of magnitude during development but, unlike the mature heart, the embryonic heart grows by hyperplasia (18). The helical arrangement of myofibers is evident at a very early stage of cardiac development and can be accelerated or delayed by manipulating the loading conditions (19). At the stage of an embryo, the primitive tubular heart develops from two layers of epithelial cells (20) (Fig. 1). The inner layer proliferates and grows toward the ventricular cavity as sheets and chords that develop into trabeculae. Cells in the outer layer proliferate and undergo progressive compaction in response to the functional needs of a growing embryo. The early embryonic heart responds to changes in its mechanical environment. Pressure overload, for example, leads to increased thickness of the trabeculae and to precocious spiraling of the trabecular architecture (18,20).

The propulsion of blood flow in an embryonic tubular heart parallels an initial isotropic electrical activation sequence that spreads from the most caudal portion of the tubular heart toward the cranially located outflow (21). Using a model of embryonic zebrafish heart tube, it has recently been suggested that this blood propulsion is not because of peristalsis but the result of dynamic suction of the tubular heart (22). Soon after the initial contractions, the process of cardiac looping begins to transform the heart into a curved tube (18). During looping, the heart tube undergoes ventral bending and torsion to create the basic pattern of the mature heart (23). Formation of torsional component of the looping promotes a change from the propulsive movements of the tubular heart to the twisting pattern seen in adult life. Further maturation of the LV wall is accompanied with emergence of a specialized His-Purkinje conduction system that progressively alters the immature base-to-apex sequence of electromechanical activation into a mature apex-to-base pattern (21).

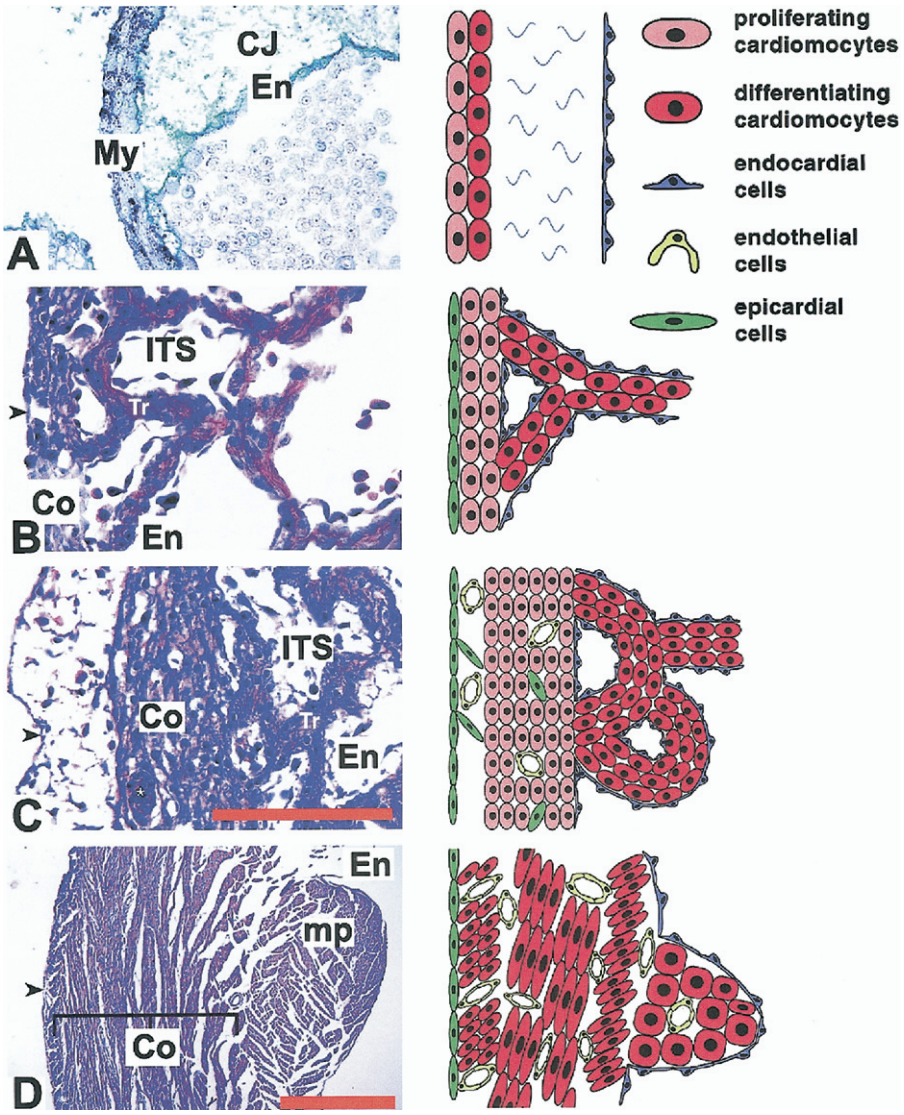

Figure 1. Embryonic development of the left ventricular wall in a chick. **(A)** The tubular myocardium (My) (2 to 3 cell layers thick) is separated from the endocardium (En) by acellular cardiac jelly (CJ). **(B)** The inner layers proliferate to form trabeculations (Tr), which are nourished by the blood circulating through the intertrabecular spaces (ITS). The outer layers proliferate and undergo compaction (Co) and are covered by epicardium **(arrowhead)**. **(C)** By the sixth embryonic day, the compact layer has thickened and is invaded by developing coronaries from the epicardial surface. **(D)** In the neonatal (day 10) heart, the multilayered compact architecture of the left ventricular wall is clearly appreciated with the innermost layer merging with the papillary muscle (mp). On the right side of each picture is a schematic drawing illustrating the major steps in development of ventricular myoarchitecture. Scale bars = **A**, **B**, **C**, 100 μm; **D**, 500 μm. Reproduced from Sedmera et al. (20) with permission.

With regard to mechanical performance, an interesting feature of an early trabeculated heart is the pattern of ventricular filling. Filling of an early embryonic looped heart occurs predominantly in late diastole, primarily because of atrial contraction, and shifts into early diastole after the addition of outer ventricular layers (24). A good correlation is seen to exist between the thickness of outer compact myocardium and the suction performance of a developing heart. A mutant mouse model with underdeveloped outer layers of myocardium shows diastolic dysfunction with diminished suction gradient and reduced force development during ejection (24). Thus, the progressive addition of outer compact spiral layers contributes to the efficient ejection and suction performance of the developing heart.

LEFT VENTRICULAR ARCHITECTURE IN ADULT LIFE

Early historic descriptions of the relation between myocardial structure and function were based on the belief that the heart comprised distinct muscle bundles that worked like skeletal muscles, with the long axis spiraling around the heart chambers (25,26). Subsequent descriptions of myocardial architecture have ranged from laminated sheets, layered fibers, and complex nested syncytium to a unique band-like arrangement (25–31). Torrent-Guasp et al. (28,29) attracted major attention in recent years to their proposed model in which the continuum of myocardial architecture was depicted in the form of a muscle band that was spatially organized into 2 distinct helicoids. Although

the model emphasized the importance of counter-directional helical anatomy in the LV, the embryological origin and existence of a unique band-like arrangement in the LV has been debated by other investigators (7,8,31).

The myocardial cells are single-nucleated and are themselves supported loosely within a continuous matrix of fibrous tissue. Groups of myocytes are surrounded by condensations of the endomysial weave, thus forming the perimysium, which aggregates a meshwork of myocytes into the so-called myofibers (31). The attachments between neighboring cells and matrix accommodates shearing between cardiac muscle fibers (32) and dynamic alterations in myocardial fiber direction during different phases of cardiac cycle (33).

Most studies have analyzed the architecture of the myocardium in transmural plugs of ventricular tissue that permit a detailed examination within a given region of myocardium (34–36). Myofiber morphology has either been described based on orientation of individual fibers or as multiple myocyte "sheet" arrangements separated by extensive "sheet-cleavage" planes. For describing the global arrangement, most studies and computational models have depicted LV myocardial architecture as a transmural continuum between 2 helical fiber geometries, where right-handed helical geometry in the subendocardial region gradually changes into left-handed geometry in the subepicardial region (33,37,38) (Fig. 2). Mathematical models have shown that this counterdirectional helical arrangement of muscle fibers in the heart is energetically efficient and is important for equal redistribution of stresses and strain in the heart (37). Incidentally, a counterdirectional arrangement of muscle fibers in the LV mirrors the structural theme that exists for propulsion in other organ systems, such as the alimentary tract, in which smooth muscles in 2 opposite directions generate peristaltic waves (39). Similarly, biophysical studies in various animals have shown the use of synergistic though inversely oriented pairs of skeletal muscles for propulsion, locomotion, or flying (40). The counterdirectional arrangement of muscle fibers helps maintain stability and minimizes energy expenditure (40).

For quantification of fiber orientation, the helix and transverse angles were introduced by Streeter et al. (27). The helix angle represents the angle between the circumferential axis and the projection of the myofiber onto the circumferential-longitudinal plane. The myofiber helix angle changes continuously from the subendocardium to the subepicardium, from a right- to a left-handed helix (Fig. 2), typically ranging from $+60^{\circ}$ at the subendocardium to -60° at the subepicardium (41). The tranverse angle represents the angle between the circumferential axis and the projection of myofiber orientation onto the radial-circumferential plane (41) and ranges between -20° to $+20^{\circ}$ (33). Le Grice et al. (42) found that collagen binds adjacent myocytes together forming layers known as lamina or sheets, which typically are 4 cells thick and separated by cleavage planes. On the basis of this finding, other investigators incorporated the helix angle (α) and the sheet angles in longitudinal radial plane (β') and circumferential radial plane (β'') in descriptions of the myofiber and sheet arrangements (43).

Figure 3 shows the arrangement of sheets and cleavage plane in the longitudinal cross-sectional plane (β'). A radial arrangement of fiber sheets and cleavage planes produces a distinct layered appearance (33). Figure 4 shows the arrangement of fiber sheets and cleavage plane in a radial cross-sectional plane (β'') taken through the mid LV and viewed from the LV base. The cross sections of the sheets within the short-axis sections diverge from the midwall. Such a characteristic appearance of myofiber arrangement can also be identified in the human LV when viewed in its short axis and was first described by Greenbaum et al. (44) and recently also reviewed by Anderson et al. (31,45). These transmural differences in orientation of muscle fibers and cleavage planes within the myocardial wall can be appreciated noninvasively using diffusion tensor magnetic resonance imaging (MRI) (Fig. 5) (46) and high-resolution ultrasonography (Video 1 and supplementary Fig 1. [see

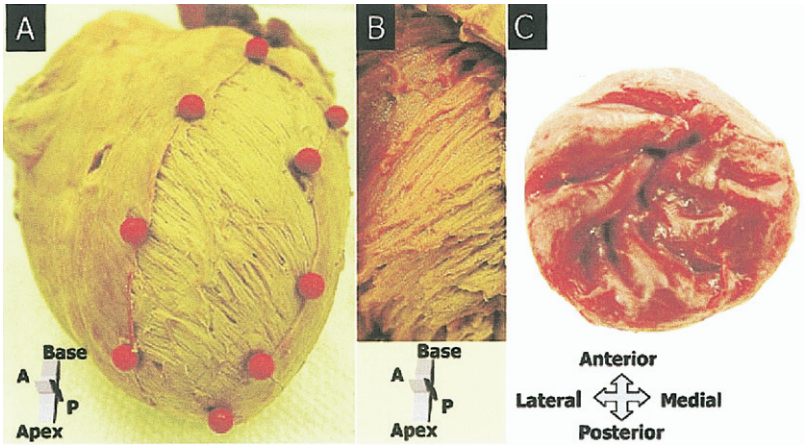

Figure 2. Helical arrangement of muscle fibers in the left ventricle of an explanted adult porcine heart. The arrangement of muscle fibers as seen in the circumferential-longitudinal plane changes from a left-handed helix in the subepicardium **(A)** to a right-handed helix in the subendocardium **(B)**. The helical arrangement of the endocardial region is also reflected in the arrangement of trabeculae near the apex **(C)**. A = anterior; P = posterior.

JACC Vol. 48, No. 10, 2006
November 21, 2006:1988–2001

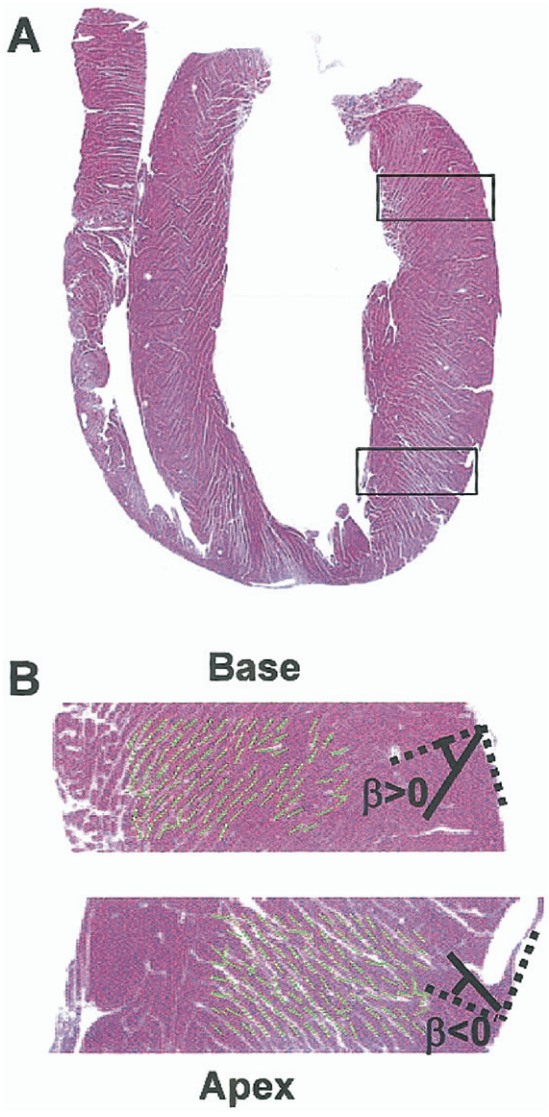

Figure 3. Arrangement of left ventricular fiber sheets and cleavage planes in long-axis slices. **(A)** Longitudinal cross section of the left ventricle fixed in diastole (hematoxylin and eosin stain). **(B)** Radial orientation of the cleavage planes and the quantification of diastolic and systolic angles of the sheets and the cleavage planes from the boxed area in **A**. Reproduced from Chen et al. (33) with permission.

Appendix]). When a high-resolution ultrasound transducer is moved over an explanted porcine heart specimen from the apex toward the base, the panning cross-sectional view as seen from the basal end of the LV shows an outer clockwise and inner counterclockwise movement of speckles due to the counterdirectional arrangement of the fiber sheets in the subendocardial and the subepicardial regions (Video 1 [see Appendix]). The predominant left-handed helical arrangement of myofibers at the LV apex can be identified by cardiac ultrasound even in a beating heart (Video 2 [see Appendix]).

ELECTRICAL SEQUENCE IN THE ADULT HEART

The fascicles of the His-Purkinje system are insulated from the surrounding muscle during their course from the crest of the septum toward the ventricular apex (21). The LV myocardial wall is, therefore, first activated at the LV endocardium in septal and anterior free wall regions, close to the LV apical endocardium (47). From these exits of the Purkinje system, the LV activation sequence travels from apex to base with small differences in activation between the septum and LV free wall (47). Pacing from the LV apex has been shown to provide a more physiologic sequence of activation and LV function than that produced with right ventricular or LV free wall stimulation (48,49).

Although electrical gradients produced by the matching sequence of ventricular depolarization results in QRS complex on surface ECG, the gradient's underlying repolarization has been widely debated. Roughly, 3 types of repolarization inhomogeneities play a role: 1) differences between the right and left ventricle; 2) differences between apex-base

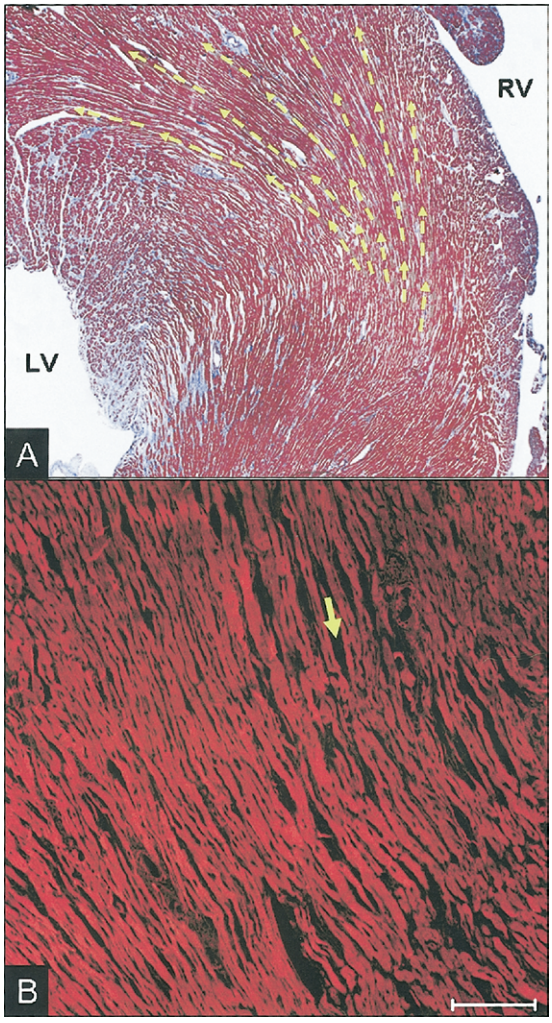

Figure 4. Cross-sectional view of a rat's left ventricle (LV) when viewed along the short axis. The cross section obtained from the midsegment of the interventricular septum has been viewed from the basal end of the LV. The fiber sheets **(dashed arrows)** are seen to diverge away from midwall (hematoxylin and eosin stain) **(A)**. The cleavage planes **(arrow)** separating the myofiber sheets are distinctly appreciated using high-resolution confocal laser scanning micrograph **(B)** magnification. Scale bar in **B** = 200 μm. RV = right ventricle.

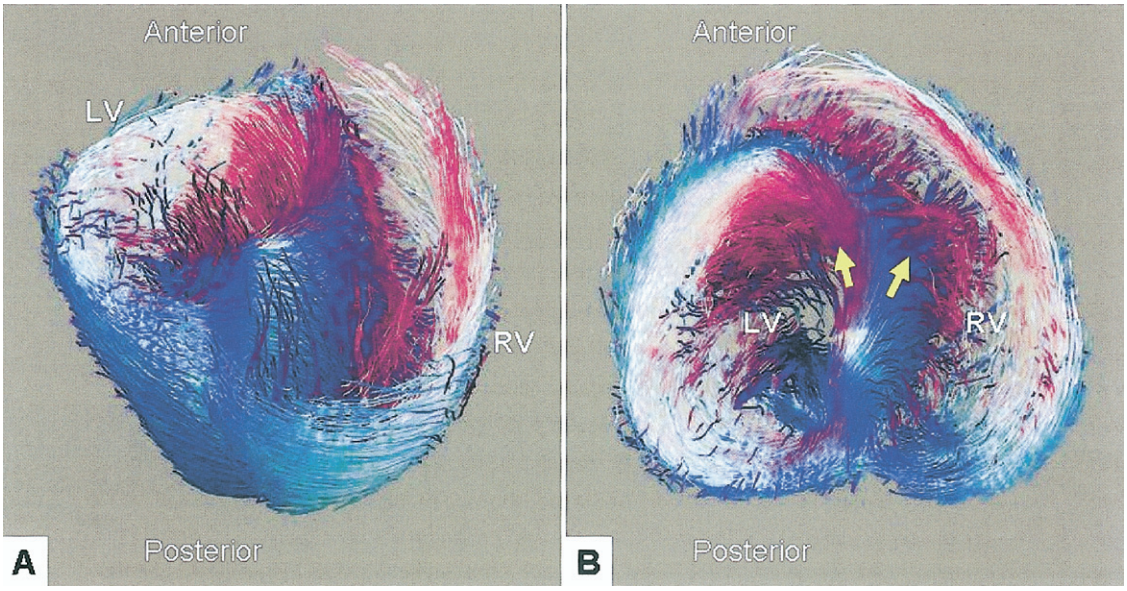

Figure 5. Assessment of cardiac muscle fiber orientation by diffusion tensor magnetic resonance imaging. In these examples **(A and B)**, scalar and tensor glyph visualization methods have been used to investigate the helical structure of the heart muscle in an explanted fixed canine heart. Right-handed helical orientation (subendocardium) is shown in shades of **purple**, and left-handed helical muscle fiber orientation (subepicardium) is shown in shades of **blue**. The cross-sectional view **(B)** has been viewed from the basal end of the left ventricle. Reproduced from Zhukov and Barr (46) with permission. LV = left ventricle; RV = right ventricle.

and anterior-posterior; and 3) transmural differences (50). In previous investigations, the presence of a repolarization gradient between the "mid-myocardial region" (M-cells) and subendocardial and subepicardial regions has been correlated with the genesis of upright T waves in ventricular wedge preparations (51). However, studies of intact hearts have failed to provide evidence for transmural differences in repolarization (52). Thus the genesis of T wave on surface electrocardiogram (ECG) may be largely due to the base-to-apex gradient with minimum contribution from the transmural gradient (50,53).

MECHANICAL SEQUENCE OF AN ADULT HEART

Isovolumic contraction. Cardiac isovolumic phases are characterized by transient changes in LV shape that produce rapid variations in regional velocities. Rushmer (54) had shown that LV geometric changes during the initial phases of systole were not isometric but were characterized by abrupt expansion of the external circumference. An advent of tissue Doppler imaging further facilitated quantification of rapid variations in regional velocities (55) during isovolumic intervals. Both open-chest experimental animal models and human studies (55–57) have reported a bidirectional movement of the LV wall during isovolumic contraction (IVC) (supplementary Figs. 2 and 3 [see Appendix]). Recent investigations from our laboratory and by others have shown that the biphasic longitudinal myocardial velocities and strain rate waveforms are consistently seen during IVC on tissue Doppler imaging (55–57) and result from a physiological asynchrony of shortening between the subendocardial and subepicardial regions (57,58).

In earlier descriptions of myocardial band hypothesis, Torrent-Guasp et al. (29) proposed that isometric contraction of the posterior basal epicardial region of the LV would result in a rigid external buttress, which could explain the inner bidirectional movement of the subendocardial region. However, recent investigations in the intact human heart have shown that electrical activation of the posterior basal epicardial region occurs around the down-sloping of the R wave or S wave on surface ECG (59). Mitral valve closure, on the other hand, occurs approximately at the peak of R wave (60,61), implying that mechanisms for closing the mitral valve are initiated within the LV even before the posterior basal epicardial region is electrically activated. Newer observations indicate that cardiac muscle activity during IVC is not isometric, and early shortening occurs within the subendocardial myofibers in the anterior wall of the LV (57,62). The shortening of the inner subendocardial fibers (right-handed helix) is accompanied with stretching of the outer subepicardial fibers (left-handed helix) (57). Stretching of activated cardiac muscle fibers produces rapid increase in myocardial stiffness (63,64). The "rigid external cylinder" of the basal epicardial loop as hypothesized by Torrent-Guasp et al. (29) may correspond to this early stiffening of the subepicardial fibers produced by transient stretching; however, this requires further confirmation in vivo. Shortening and stretching are reciprocal deformations that satisfy isovolumic mechanics, that is, shortening in one direction is accompanied with stretching of the orthogonal direction (57). Stretching of myofibers during IVC is also important in initiating "stretch activation response," an intrinsic length-sensing mechanism that allows muscle to adjust the force and duration of subsequent shortening

(65–67). This has recently been proposed as the main basis of the Frank-Starling mechanism of the heart (68). Stretching a myocyte that has been electrically activated increases the force of subsequent shortening due to strain of attached cross bridges and acceleration of cross-bridge cycling kinetics (69).

The papillary muscles are among the earliest portions of the ventricle that are electrically stimulated. However, during IVC, despite the electrical signal to contract, the papillary muscles also are stretched during IVC and early period of systole while other portions of the ventricle are contracting (62,67,70). This motion has been attributed to the increasing intraventricular pressure in early systole that leads to closure of the mitral valve leaflets with increasing tension on the chordae, which causes stretching of the papillary muscles (67,70).

Ejection phase. Myocardial deformation during ejection demonstrates extensive transmural tethering (71) such that subendocardial and subepicardial regions undergo simultaneous shortening along the fiber and cross-fiber direction during ejection (57,72). Subendocardial strains are higher in magnitude than subepicardial strains (Fig. 6) (53). Within subendocardium, the magnitude of circumferential strains during ejection exceeds that of longitudinal strains (13) (Figs. 6 and 7). With regard to the timing, longitudinal shortening strains for both regions show an apex-to-base gradient, so that successive shortenings are reached earlier at apex and midsegments compared to the LV base (57,72). Thus, the direction of LV mechanical shortening parallels the apex-to-base direction of electrical activation (47). Studies of canine (73) and children's (48) hearts also have shown that an apex-to-base direction of LV pacing yields a more physiologic sequence of activation and LV function.

Previous tissue Doppler image analyses in the apex-to-base direction reported a velocity gradient but nearly uniform strain and strain-rate gradients. Recent investigations using either direct sonomicrometry (53) or indirect measurement by MRI tagging (13) have reported higher shortening strains within the LV apex. Results of Doppler strain measurements are dependent on the angle between the scan axis and tissue and may have inherent limitations in accurately measuring deformation from curved regions of LV, particularly near the apex. Measurements with a recently developed technique of measuring 2-dimenstional strains by

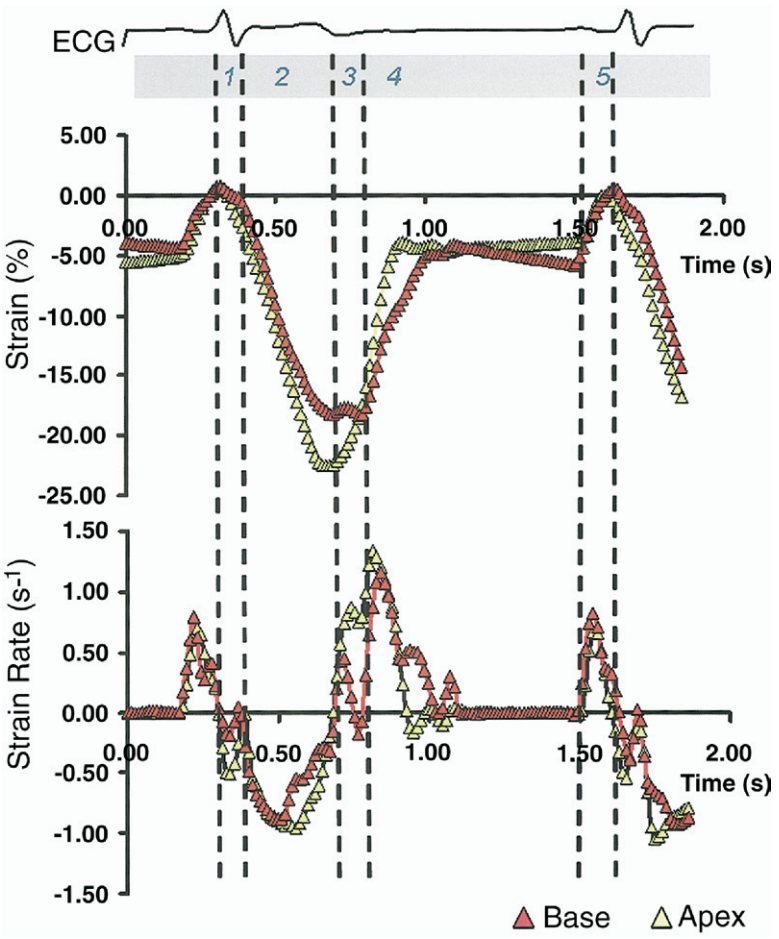

Figure 6. Longitudinal deformation of the anterior wall of the left ventricle by 2-dimensional speckle tracking of B-mode ultrasound images (2-dimensional strain). Longitudinal shortening starts during isovolumic contraction period and occurs earlier in the apex as compared with the base. Shortening-lengthening crossover of the basal anteroseptal segment is delayed until the end of isovolumic relaxation. Phase 1, isovolumic contraction; 2, ejection; 3, isovolumic relaxation; 4, early diastole; 5, late diastole. ECG = electrocardiogram.

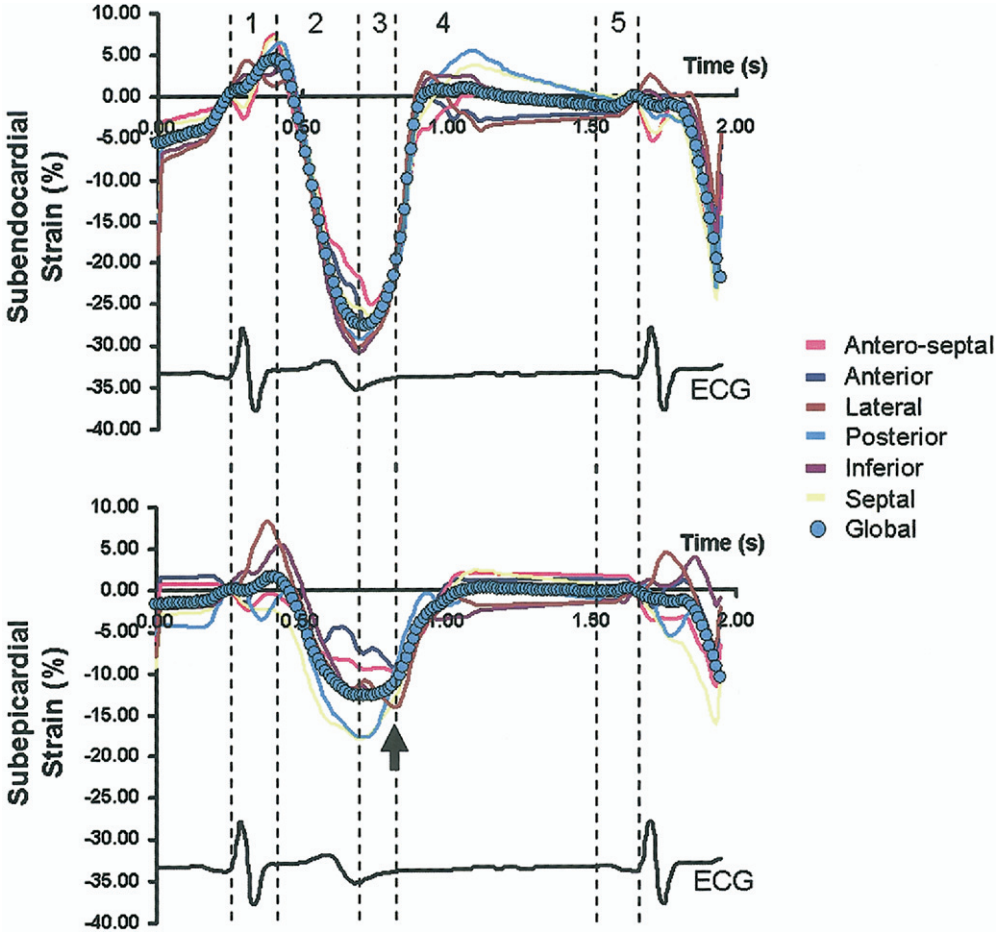

Figure 7. Circumferential deformation of the subendocardial and subepicardial regions of left ventricular apex by 2-dimensional speckle tracking of B-mode ultrasound images (2-dimensional strain). Note the presence of positive strains (lengthening) during the phase of isovolumic contraction. Note the higher circumferential strains of the subendocardial regions as compared with the subepicardial region. Peak shortening in some segments of the subepicardial region extends beyond the timing of aortic valve closure (postsystolic shortening, **arrow**). Phases 1 to 5 are described in the legend to Figure 6. ECG = electrocardiogram.

speckle tracking of B-mode ultrasound images (74) also suggest that radial and longitudinal strains and strain rates are higher in the apex compared to the base (Fig. 6, Video 3 [see Appendix]) (75,76).

Isovolumic relaxation and postsystolic shortening. Two types of mechanical gradients operate during isovolumic relaxation (IVR): apex-to-base and transmural gradients (Figs. 6 and 7). Near the LV apex, shortening of the subepicardium (left-handed helix) continues beyond aortic valve closure and is accompanied with lengthening of the subendocardial layer (right-handed helix) (53,72). Near the LV base, lengthening of myocardial wall occurs along the left-handed helical subepicardial fiber direction and is accompanied with shortening and shear along the subendocardial fiber sheets (i.e., right-handed fibers) (36,53). Changes in LV cavity volume follow the deformation pattern of the subendocardium, with enlargement of the LV cavity at the apex.

Longitudinal and circumferential shortening of the myocardial wall during the IVR period has been reported in normal human subjects (77,78). Zwanenburg et al. (77) timed cardiac contraction in healthy subjects with high-temporal-resolution MRI myocardial tagging and reported that several segments in the lateral wall and in the basal regions contracted circumferentially beyond aortic valve closure (Fig. 8). The occurrence of longitudinal postsystolic shortening in healthy subjects was reported also by Voigt et al. (78). Postsystolic shortening as a physiological phenomenon may be explained on the basis of synergistic movements that occur during IVR, that is, lengthening of the LV segment in one direction is accompanied with shortening in the other direction. Recent observations in beating porcine hearts indicate that a component of this reciprocal shortening occurs circumferentially near the apex and is linked with longer repolarization intervals. Normal postsystolic contraction of the LV provides an apex-to-base and transmural gradient of deformation that may help in rapidly restoring the geometry of LV cavity in early diastole (53,72). Delayed force development is predominantly seen in regions that undergo prestretching during IVC, that is, stretch activation, and results from recruitment of additional cross bridges to sustain a state of prolonged force generation (69).

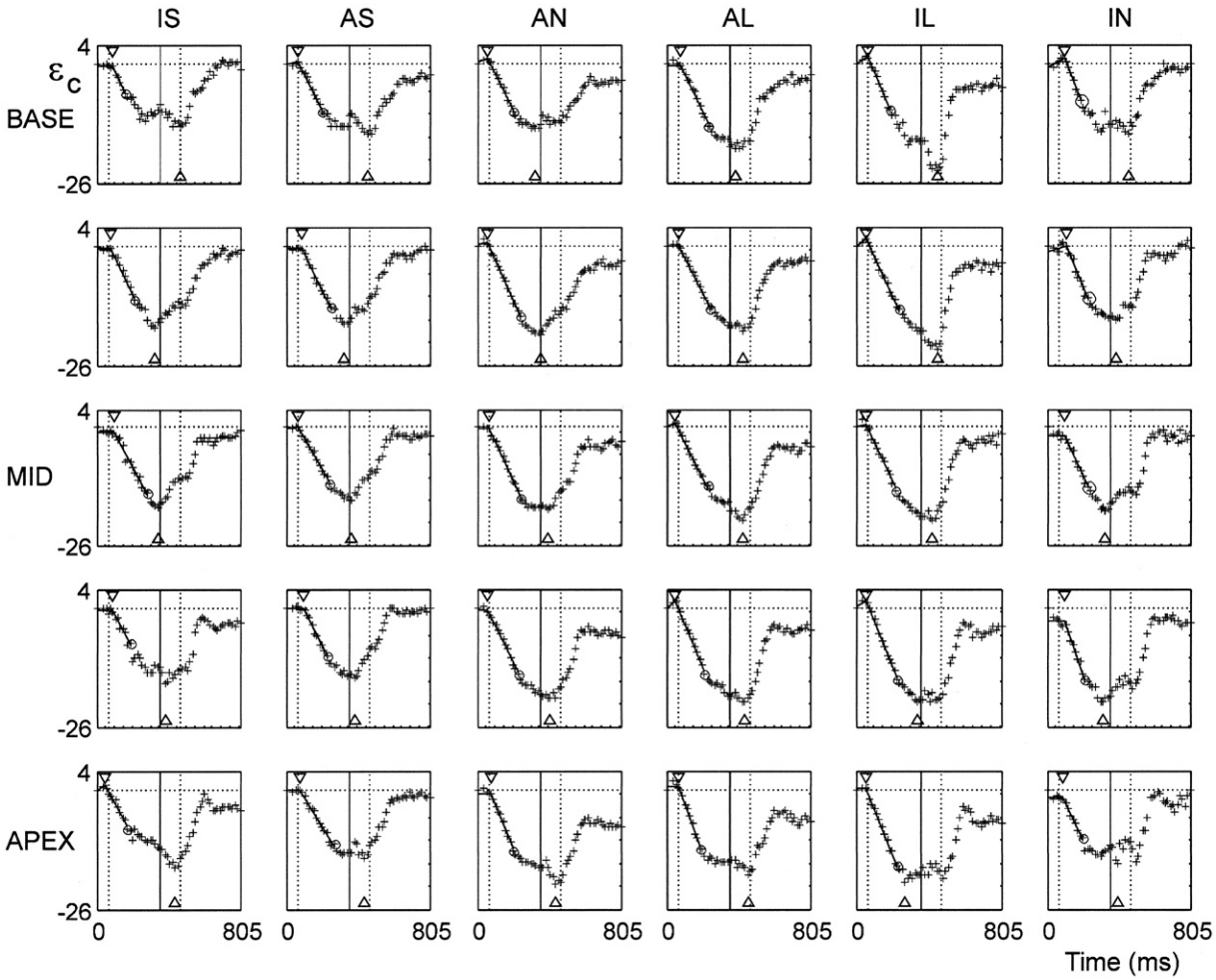

Figure 8. Time sequence of circumferential shortening in a healthy subject by tagged magnetic resonance imaging. Several segments contract beyond aortic valve closure. + = measured data points; − = fitted line model to data for estimating T_{onset}; circled + = end point of data used in the fit; upside-down triangles = estimated T_{onset}; triangles = T_{peak}. The vertical lines denote, from **left to right**, the moment of aortic valve opening **(dashed)**, aortic valve closure **(solid)**, and mitral valve opening **(dashed)**. AL = anterolateral; AN = anterior; AS = antero-septal; IL = inferolateral; IN = inferior; IS = inferoseptal. Reproduced from Zwanenburg et al. (77) with permission.

Coexistence of shortening and lengthening deformations within the LV wall during the isovolumic phases (57,58) makes "contraction" and "relaxation" terms misleading for defining the corresponding phases (IVC and IVR, respectively). Instead, the terms of "isovolumetric ventricular contraction" or "systolic ventricular filling" due to a muscular mechanism recently have been suggested (79). However, published reports are inconsistent with regard to the definition of "systole" and "diastole" (80). Even Wiggers, who originally defined the phases of cardiac cycle, found it most difficult to correlate end ejection with valve closure and to delineate exactly the moment when "systole" ceases and when relaxation of muscle and ventricle starts (80). He admitted that this intermediary interval belongs, strictly speaking, neither to the period of systole nor to that of diastole (80). To avoid this uncertainty, we propose using the term "'pre- and postejection" isovolumic intervals for providing more succinct information because such definition can include existence of simultaneous myocardial shortening or lengthening within the LV wall.

Left ventricular thickening. Continuum mechanics would suggest that continuity of wall materials is all that is required for LV wall thickening. Shortening in longitudinal and circumferential direction would result in thickeneing in the radial direction for conserving mass. However, LV wall thickening is not a resultant of simple shortening of individual myocytes in concert but an effect of shearing of groups of myocytes across each other (Video 4 [see Appendix]). Transmural shearing results from sliding and rearrangement of myofiber sheets along cleavage planes during the cardiac cycle (33,42,81). Rademakers et al. (82) used MR myocardial tagging and showed that cross-fiber strain was near zero at the epicardium but was large at the endocardium and increased from base to apex. This study concluded that the primary source of myocardial wall thickening was the interaction between the different layers of the myocardium (82). The transmural variations in radial deformation depend upon the regional differences in activation and electromechanical coupling of myocardial layers. Anatomical M-mode echocardiography and Doppler can be

used for timing the transmural differences in the onset and peaking of radial motion during different phases of cardiac cycle (Fig. 9).

Left ventricular twist. In the past, dynamics of LV rotation were assessed by implanting multiple radioopaque markers and biplane cine angiography (83,84). Currently, LV twist can be assessed noninvasively by MRI and 2-dimensional echocardiography (85). Recently introduced 2-dimensional strain echocardiography allows rapid and accurate measurement of regional twist angles or rotation (86). Rotation is conventionally viewed from the apical end of the LV, with clockwise and counterclockwise rotations shown in negative and positive degrees respectively. During IVC, the LV apex shows brief clockwise rotation (supplementary Fig. 4 [see Appendix]) (87,88). This is explained by the predominant mechanical activity that develops along the right-handed helical direction during IVC because of shortening of the subendocardial region (89). During ejection, the apical rotation reverses becoming counterclockwise and the direction corresponds with the orientation of the left-handed helical subepicardial myofibers. Beyar et al. (84) demonstrated for the first time in a canine model that a major component of untwisting (clockwise rotation) occurred during the IVR and early period of diastole. Subsequently, in another canine experimental study, it was shown that untwisting of LV apex was initiated within IVR following the first 20 ms of aortic valve closure and approximately 50% of untwisting occurred before mitral valve opening (supplementary Fig. 4 [see Appendix]) (90).

Rotation of the LV base is opposite to that of the apex but is significantly lower in its magnitude. During IVC, there is a brief counter-clockwise rotation due to the mechanical activity of the subendocardial fibers, which is followed by clockwise rotation (twist) during ejection when the subepicardal myofibers dominate the direction of LV rotation. The counterdirectional rotation of the LV apex

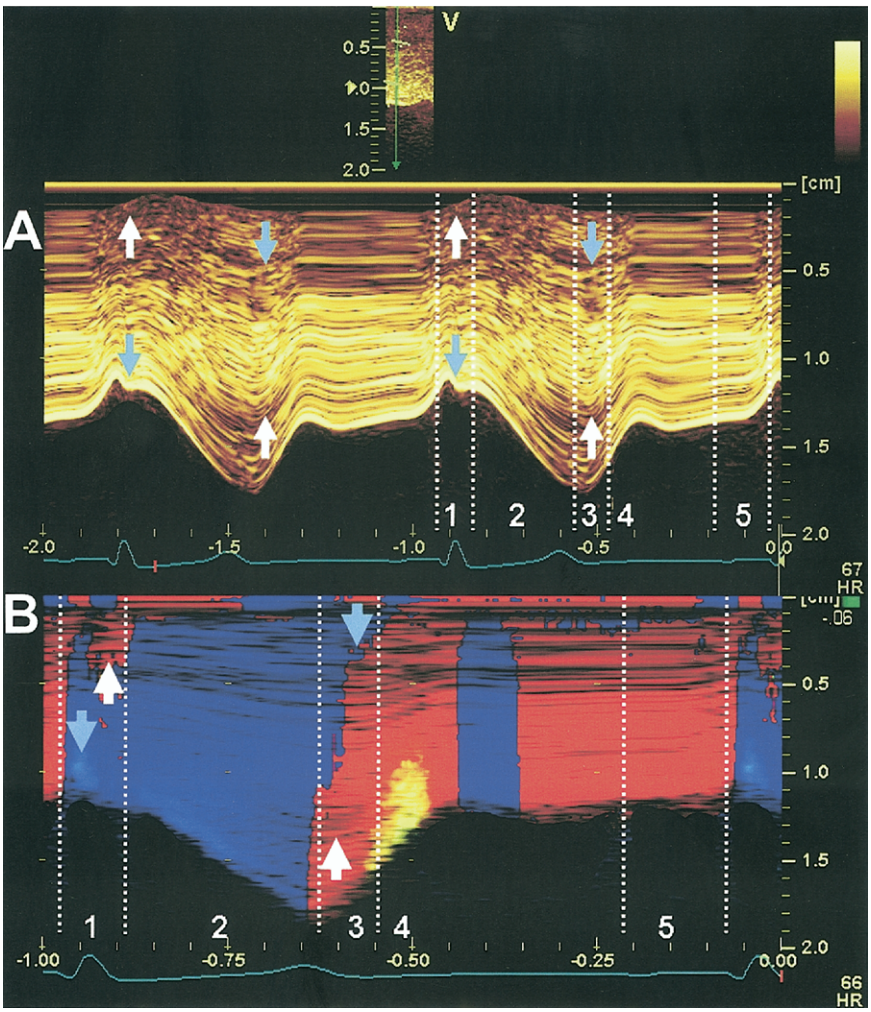

Figure 9. Direct in vivo imaging of anterior wall of a beating porcine left ventricle using high-resolution linear array transducer (10 MHz). **(A)** Anatomic M-mode imaging of the different layers of anterior segment of left ventricular apex at high temporal resolution (250 frames/s). During isovolumic contraction, the endocardium moves toward the cavity **(blue arrows)** and is accompanied with a reciprocal outward movement of the subepicardium **(white arrows)**. A reverse pattern of movement is seen during isovolumic relaxation. These reciprocal movements of the subendocardial and subepicardial regions also are seen in tissue Doppler imaging, in the form of simultaneous **red** and **blue** colors within the inner and outer layers of the same segment of the myocardial wall during isovolumic contraction and vice versa during isovolumic relaxation **(B)**. Phases 1 to 5 are described in the legend to Figure 6.

with respect to the base results in a "wringing" movement during ejection. The pattern of net LV twist in which the apex and the base rotate in different directions has been explained on the basis of varying spiral myofiber architecture of the apical and basal region and apex-to-base and transmural gradients in myosin phosphorylation (67,91).

LEFT VENTRICULAR MECHANICAL SEQUENCE SYNCHRONIZES THE DIRECTION OF BLOOD FLOW

Magnetic resonance imaging (92) and echocardiography (61,93) can be used for deciphering the 2-dimensional features of LV intracavitary flow during different phases of cardiac cycle. During high temporal resolution contrast echocardiography (Video 6 [see Appendix]), bubbles are tracked in time and space for creating trajectories of blood flow in 2 dimensions (61,93). Figure 10 shows the direction of blood flow during each phase of the cardiac cycle analyzed by echo contrast particle imaging velocimetry. After the onset of a Q-wave on the surface ECG, just before the mitral valve closure, the blood flow accelerates in the apex-to-base direction, paralleling the apex-to-base direction of electromechanical activation. This accelerated stream unites with a large vortex that is formed across the anterior edge of a closing anterior mitral leaflet (Video 6 [see Appendix]). The forced acceleration of blood in the direction of LV outflow before the opening of the aortic valve correlates temporally with the reshaping movement of the LV wall seen during IVC. Contraction in one direction (right-handed helix) displaces blood, stretching the orthogonal direction (left-handed helix) during the isovolumic period. Because the left handed helix direction faces the outflow, blood is displaced towards the LV outflow before the aortic valve opening (Video 6 [see Appendix]). Further propulsion of blood from the LV cavity results into ejection. IVR is characterized with rapid base-to-apex reversal of blood flow (61,94) (Video 5 [see Appendix]). This explains the physiologic significance of early endocardial relaxation and opening of the LV cavity near the apex during IVR. This base-to-apex suction of blood during IVR helps to accommodate a greater base-to-apex surge of blood flow once the mitral valve opens during early diastolic filling. Both early and late diastolic flows are characterized with

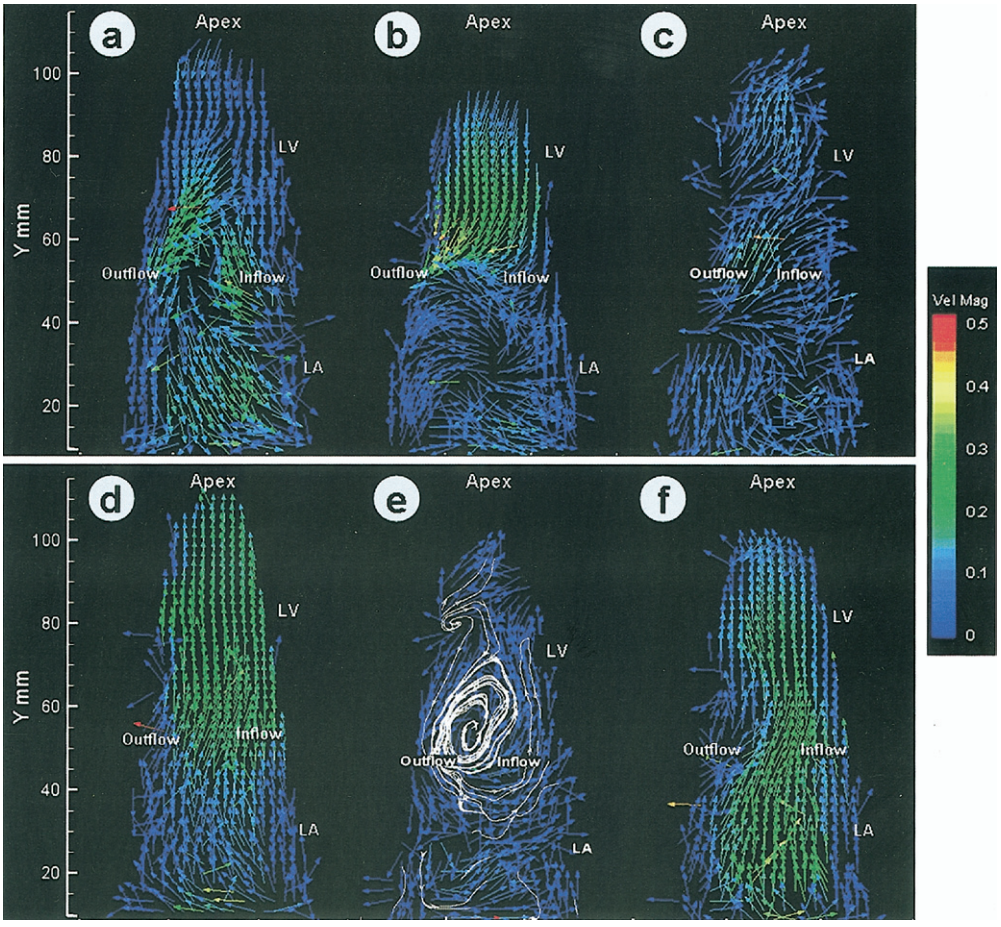

Figure 10. Digital particle image velocimetry profiles of left ventricular flow during each phase of the cardiac cycle. Under specific conditions of dilution and administration to blood circulation, the echo contrast particles (microbubbles) can be tracked for calculating vectors and trajectories of flow within a 2-dimensional ultrasound scan plane. The ensemble-averaged velocity magnitudes are superimposed on the vector fields during isovolumic contraction **(a)**, ejection **(b)**, isovolumic relaxation **(c)**, early diastole **(d)**, diastasis **(e)**, and late diastole **(f)**. Note the apex-to-base redirection of blood flow during isovolumic contraction with formation of a dynamic vortex across the inflow-outflow region and the base-to-apex reversal of blood flow during isovolumic relaxation. LA = left atrium; LV = left ventricle. Reproduced from Sengupta et al. (61).

formation of a large anterior vortex across the anterior mitral leaflet and a small posterior vortex across the posterior mitral leaflet (61,95). Intracavitary blood flow seen during the different phases of the cardiac cycle thus provides enhanced understanding about the significance of the apex-to-base sequence of mechanical activation. Since inflow and outflow of the LV are found closely aligned at the "top" of the ventricle, apex-to-base activation and contraction of the subendocardial fibers contributes to acceleration of blood flow in the direction of the aortic outlet for optimal ejection (7,61).

FINAL COMMENTS

We have reviewed the LV myofiber architecture with the eletromechanical activation and intracavitary blood flow sequence and provided the reasoning for complex deformation of a beating heart observed in vivo. The short-lasting highly localized deformations and the physiologic asynchrony of cardiac deformation can be deciphered accurately only when analyzed in reference to the structural anisotropy of the underlying myocardial architecture. This information became available with the advent of high temporal resolution imaging methods and is fundamental for understanding cardiac physiology, optimization of cardiac therapies and planning of surgical procedures used for restoring the LV geometry (96). Another important objective in attempting to discern the link between the structure and function of a beating heart is to develop accurate computational models that can assimilate all imaging information for planning of proper therapeutic strategies for a given individual patient (97). Understanding the cardiac structure–function relationship will also be essential for generating true anatomical constructs and scaffolds that would guide the emerging field of cardiac tissue engineering in time for designing future components of a "bioartificial heart" (98).

Reprint requests and correspondence: Dr. Bijoy K. Khandheria, Division of Cardiovascular Diseases, Mayo Clinic, 13400 East Shea Boulevard, Scottsdale, Arizona 85259. E-mail: khandheria@mayo.edu.

REFERENCES

1. Young JB. The global epidemiology of heart failure. Med Clin North Am 2004;88:1135–43, ix.
2. Thom T, Haase N, Rosamond W, et al. Heart disease and stroke statistics—2006 update: a report from the American Heart Association Statistics Committee and Stroke Statistics Subcommittee. Circulation 2006;113:e85–151.
3. Mann DL, Bristow MR. Mechanisms and models in heart failure: the biomechanical model and beyond. Circulation 2005;111:2837–49.
4. Buckberg GD, Weisfeldt ML, Ballester M, et al. Left ventricular form and function: scientific priorities and strategic planning for development of new views of disease. Circulation 2004;110:e333–6.
5. Buckberg GD. Architecture must document functional evidence to explain the living rhythm. Eur J Cardiothorac Surg 2005;27:202–9.
6. Lunkenheimer PP, Redmann K, Anderson RH. Further discursions concerning the unique myocardial band. Eur J Cardiothorac Surg 2005;28:779.
7. Sedmera D. Form follows function: developmental and physiological view on ventricular myocardial architecture. Eur J Cardiothorac Surg 2005;28:526–8.
8. Criscione JC, Rodriguez F, Miller DC. The myocardial band: simplicity can be a weakness. Eur J Cardiothorac Surg 2005;28:363–4.
9. Prinzen FW, Augustijn CH, Allessie MA, Arts T, Delhaas T, Reneman RS. The time sequence of electrical and mechanical activation during spontaneous beating and ectopic stimulation. Eur Heart J 1992;13:535–43.
10. Helm RH, Leclercq C, Faris OP, et al. Cardiac dyssynchrony analysis using circumferential versus longitudinal strain: implications for assessing cardiac resynchronization. Circulation 2005;111:2760–7.
11. Smiseth OA, Remme EW. Regional left ventricular electric and mechanical activation and relaxation. J Am Coll Cardiol 2006;47:173–4.
12. Rankin JS, McHale PA, Arentzen CE, Ling D, Greenfield JC Jr., Anderson RW. The three-dimensional dynamic geometry of the left ventricle in the conscious dog. Circ Res 1976;39:304–13.
13. Bogaert J, Rademakers FE. Regional nonuniformity of normal adult human left ventricle. Am J Physiol Heart Circ Physiol 2001;280:H610–20.
14. Yip G, Abraham T, Belohlavek M, Khandheria BK. Clinical applications of strain rate imaging. J Am Soc Echocardiogr 2003;16:1334–42.
15. Lorenz CH, Pastorek JS, Bundy JM. Delineation of normal human left ventricular twist throughout systole by tagged cine magnetic resonance imaging. J Cardiovasc Magn Reson 2000;2:97–108.
16. Henson RE, Song SK, Pastorek JS, Ackerman JJ, Lorenz CH. Left ventricular torsion is equal in mice and humans. Am J Physiol Heart Circ Physiol 2000;278:H1117–23.
17. Delhaas T, Kotte J, van der Toorn A, Snoep G, Prinzen FW, Arts T. Increase in left ventricular torsion-to-shortening ratio in children with valvular aortic stenosis. Magn Reson Med 2004;51:135–9.
18. Taber LA. Biomechanics of cardiovascular development. Annu Rev Biomed Eng 2001;3:1–25.
19. Tobita K, Garrison JB, Liu LJ, Tinney JP, Keller BB. Three-dimensional myofiber architecture of the embryonic left ventricle during normal development and altered mechanical loads. Anat Rec A Discov Mol Cell Evol Biol 2005;283:193–201.
20. Sedmera D, Pexieder T, Vuillemin M, Thompson RP, Anderson RH. Developmental patterning of the myocardium. Anat Rec 2000;258:319–37.
21. Reckova M, Rosengarten C, deAlmeida A, et al. Hemodynamics is a key epigenetic factor in development of the cardiac conduction system. Circ Res 2003;93:77–85.
22. Forouhar AS, Liebling M, Hickerson A, et al. The embryonic vertebrate heart tube is a dynamic suction pump. Science 2006;312:751–3.
23. Nerurkar NL, Ramasubramanian A, Taber LA. Morphogenetic adaptation of the looping embryonic heart to altered mechanical loads. Dev Dyn 2006;235:1822–9.
24. Ishiwata T, Nakazawa M, Pu WT, Tevosian SG, Izumo S. Developmental changes in ventricular diastolic function correlate with changes in ventricular myoarchitecture in normal mouse embryos. Circ Res 2003;93:857–65.
25. Mall F. On the muscular architecture of the ventricles of the human heart. Am J Anat 1911;11:211–66.
26. MacCallum JB. On the muscular architecture and growth of the ventricles of the heart. Johns Hopkins Hosp Rep 1900;9:307–35.
27. Streeter DD Jr., Spotnitz HM, Patel DP, Ross J Jr., Sonnenblick EH. Fiber orientation in the canine left ventricle during diastole and systole. Circ Res 1969;24:339–47.
28. Torrent-Guasp FF, Whimster WF, Redmann K. A silicone rubber mould of the heart. Technol Health Care 1997;5:13–20.
29. Torrent-Guasp F, Ballester M, Buckberg GD, et al. Spatial orientation of the ventricular muscle band: physiologic contribution and surgical implications. J Thorac Cardiovasc Surg 2001;122:389–92.
30. Bovendeerd PH, Huyghe JM, Arts T, van Campen DH, Reneman RS. Influence of endocardial-epicardial crossover of muscle fibers on left ventricular wall mechanics. J Biomech 1994;27:941–51.
31. Anderson RH, Ho SY, Redmann K, Sanchez-Quintana D, Lunkenheimer PP. The anatomical arrangement of the myocardial cells making up the ventricular mass. Eur J Cardiothorac Surg 2005;28:517–25.

32. McCulloch AD, Omens JH. Myocyte shearing, myocardial sheets, and microtubules. Circ Res 2006;98:1–3.
33. Chen J, Liu W, Zhang H, et al. Regional ventricular wall thickening reflects changes in cardiac fiber and sheet structure during contraction: quantification with diffusion tensor MRI. Am J Physiol Heart Circ Physiol 2005;289:H1898–907.
34. Arts T, Costa KD, Covell JW, McCulloch AD. Relating myocardial laminar architecture to shear strain and muscle fiber orientation. Am J Physiol Heart Circ Physiol 2001;280:H2222–9.
35. Takayama Y, Costa KD, Covell JW. Contribution of laminar myofiber architecture to load-dependent changes in mechanics of LV myocardium. Am J Physiol Heart Circ Physiol 2002;282:H1510–20.
36. Ashikaga H, Criscione JC, Omens JH, Covell JW, Ingels NB Jr. Transmural left ventricular mechanics underlying torsional recoil during relaxation. Am J Physiol Heart Circ Physiol 2004;286: H640–7.
37. Vendelin M, Bovendeerd PH, Engelbrecht J, Arts T. Optimizing ventricular fibers: uniform strain or stress, but not ATP consumption, leads to high efficiency. Am J Physiol Heart Circ Physiol 2002;283: H1072–81.
38. Nielsen PM, Le Grice IJ, Smaill BH, Hunter PJ. Mathematical model of geometry and fibrous structure of the heart. Am J Physiol 1991; 260:H1365–78.
39. Grider JR. Reciprocal activity of longitudinal and circular muscle during intestinal peristaltic reflex. Am J Physiol Gastrointest Liver Physiol 2003;284:G768–75.
40. Dickinson MH, Farley CT, Full RJ, Koehl MA, Kram R, Lehman S. How animals move: an integrative view. Science 2000;288:100–6.
41. Geerts L, Bovendeerd P, Nicolay K, Arts T. Characterization of the normal cardiac myofiber field in goat measured with MR-diffusion tensor imaging. Am J Physiol Heart Circ Physiol 2002;283:H139–45.
42. Le Grice IJ, Takayama Y, Covell JW. Transverse shear along myocardial cleavage planes provides a mechanism for normal systolic wall thickening. Circ Res 1995;77:182–93.
43. Costa KD, May-Newman K, Farr D, O'Dell WG, McCulloch AD, Omens JH. Three-dimensional residual strain in midanterior canine left ventricle. Am J Physiol 1997;273:H1968–76.
44. Greenbaum RA, Ho SY, Gibson DG, Becker AE, Anderson RH. Left ventricular fibre architecture in man. Br Heart J 1981;45:248–63.
45. Anderson RH, Ho SY, Sanchez-Quintana D, Redmann K, Lunkenheimer PP. Heuristic problems in defining the three-dimensional arrangement of the ventricular myocytes. Anat Rec A Discov Mol Cell Evol Biol 2006;288:579–86.
46. Zhukov L, Barr AH. Heart-muscle fiber reconstruction from diffusion tensor MRI. Proceedings of the 14th IEEE Visualization 2003. October 19–24, 2003:597–602.
47. Scher AM. Studies of the electrical activity of the ventricles and the origin of the QRS complex. Acta Cardiol 1995;50:429–65.
48. Vanagt WY, Verbeek XA, Delhaas T, et al. Acute hemodynamic benefit of left ventricular apex pacing in children. Ann Thorac Surg 2005;79:932–6.
49. Vanagt WY, Verbeek XA, Delhaas T, Mertens L, Daenen WJ, Prinzen FW. The left ventricular apex is the optimal site for pediatric pacing: correlation with animal experience. Pacing Clin Electrophysiol 2004;27:837–43.
50. Opthof T. In vivo dispersion in repolarization and arrhythmias in the human heart. Am J Physiol Heart Circ Physiol 2006;290:H77–8.
51. Antzelevitch C. Transmural dispersion of repolarization and the T wave. Cardiovasc Res 2001;50:426–31.
52. Janse MJ, Sosunov EA, Coronel R, et al. Repolarization gradients in the canine left ventricle before and after induction of short-term cardiac memory. Circulation 2005;112:1711–8.
53. Sengupta PP, Khandheria BK, Korinek J, et al. Apex-to-base dispersion in regional timing of left ventricular shortening and lengthening. J Am Coll Cardiol 2006;47:163–72.
54. Rushmer R. Initial phase of ventricular systole: asynchronous contraction. Am J Physiol 1956;184:188–94.
55. Lind B, Nowak J, Cain P, Quintana M, Brodin LA. Left ventricular isovolumic velocity and duration variables calculated from colour-coded myocardial velocity images in normal individuals. Eur J Echocardiogr 2004;5:284–93.
56. Edvardsen T, Urheim S, Skulstad H, Steine K, Ihlen H, Smiseth OA. Quantification of left ventricular systolic function by tissue Doppler echocardiography: added value of measuring pre- and postejection velocities in ischemic myocardium. Circulation 2002;105:2071–7.
57. Sengupta PP, Khandheria BK, Korinek J, Wang J, Belohlavek M. Biphasic tissue Doppler waveforms during isovolumic phases are associated with asynchronous deformation of subendocardial and subepicardial layers. J Appl Physiol 2005;99:1104–11.
58. Goetz WA, Lansac E, Lim HS, Weber PA, Duran CM. Left ventricular endocardial longitudinal and transverse changes during isovolumic contraction and relaxation: a challenge. Am J Physiol Heart Circ Physiol 2005;289:H196–201.
59. Ramanathan C, Jia P, Ghanem R, Ryu K, Rudy Y. Activation and repolarization of the normal human heart under complete physiological conditions. Proc Natl Acad Sci U S A 2006;103:6309–14.
60. Kjaergaard J, Hassager C, Oh JK, Kristensen JH, Berning J, Sogaard P. Measurement of cardiac time intervals by Doppler tissue M-mode imaging of the anterior mitral leaflet. J Am Soc Echocardiogr 2005;18:1058–65.
61. Sengupta PP, Khandheria BK, Korinek J, et al. Left ventricular isovolumic flow sequence during sinus and paced rhythms: new insights from use of high-resolution doppler and ultrasonic digital particle imaging velocimetry. J Am Coll Cardiol 2007. In press.
62. Buckberg GD, Castella M, Gharib M, Saleh S. Structure/function interface with sequential shortening of basal and apical components of the myocardial band. Eur J Cardiothorac Surg 2006;29 Suppl 1:S75–97.
63. Yin FC, Yamada H. The effects of left ventricular stretch versus cavity pressure on intramyocardial pressure. Cardiovasc Res 1997;34:299–305.
64. Campbell KS, Patel JR, Moss RL. Cycling cross-bridges increase myocardial stiffness at submaximal levels of Ca2+ activation. Biophys J 2003;84:3807–15.
65. Stelzer JE, Larsson L, Fitzsimons DP, Moss RL. Activation dependence of stretch activation in mouse skinned myocardium: implications for ventricular function. J Gen Physiol 2006;127:95–107.
66. Campbell KB, Chandra M. Functions of stretch activation in heart muscle. J Gen Physiol 2006;127:89–94.
67. Davis JS, Hassanzadeh S, Winitsky S, et al. The overall pattern of cardiac contraction depends on a spatial gradient of myosin regulatory light chain phosphorylation. Cell 2001;107:631–41.
68. Fukuda N, Granzier HL. Titin/connectin-based modulation of the Frank-Starling mechanism of the heart. J Muscle Res Cell Motil 2005;26:319–23.
69. Stelzer JE, Dunning SB, Moss RL. Ablation of cardiac myosin-binding protein-C accelerates stretch activation in murine skinned myocardium. Circ Res 2006;98:1212–8.
70. Semafuko WE, Bowie WC. Papillary muscle dynamics: in situ function and responses of the papillary muscle. Am J Physiol 1975; 228:1800–7.
71. McCulloch AD, Sung D, Wilson JM, Pavelec RS, Omens JH. Flow-function relations during graded coronary occlusions in the dog: effects of transmural location and segment orientation. Cardiovasc Res 1998;37:636–45.
72. Buckberg GD, Castella M, Gharib M, Saleh S. Active myocyte shortening during the "isovolumetric relaxation" phase of diastole is responsible for ventricular suction; 'systolic ventricular filling.' Eur J Cardiothorac Surg 2006;29 Suppl 1:S98–106.
73. Peschar M, de Swart H, Michels KJ, Reneman RS, Prinzen FW. Left ventricular septal and apex pacing for optimal pump function in canine hearts. J Am Coll Cardiol 2003;41:1218–26.
74. Korinek J, Wang J, Sengupta PP, et al. Two-dimensional strain—a Doppler-independent ultrasound method for quantitation of regional deformation: validation in vitro and in vivo. J Am Soc Echocardiogr 2005;18:1247–53.
75. Sukmawan R, Watanabe N, Toyota E, et al. Application of novel echocardiographic two-dimensional tracking system to define regional heterogeneity of radial and longitudinal myocardial strain and strain-rate (abstr). Circulation 2005;112:2561.
76. Serri K, Reant P, Lafitte M, et al. Global and regional myocardial function quantification by two-dimensional strain: application in hypertrophic cardiomyopathy. J Am Coll Cardiol 2006;47:1175–81.
77. Zwanenburg JJ, Gotte MJ, Kuijer JP, Heethaar RM, van Rossum AC, Marcus JT. Timing of cardiac contraction in humans mapped by high-temporal-resolution MRI tagging: early onset and late peak of

shortening in lateral wall. Am J Physiol Heart Circ Physiol 2004;286: H1872–80.
78. Voigt JU, Lindenmeier G, Exner B, et al. Incidence and characteristics of segmental postsystolic longitudinal shortening in normal, acutely ischemic, and scarred myocardium. J Am Soc Echocardiogr 2003;16: 415–23.
79. Buckberg GD. Rethinking the cardiac helix—a structure/function journey: overview. Eur J Cardiothorac Surg 2006;29 Suppl 1:S2–3.
80. Brutsaert DL, Sys SU. Relaxation and diastole of the heart. Physiol Rev 1989;69:1228–315.
81. Costa KD, Takayama Y, McCulloch AD, Covell JW. Laminar fiber architecture and three-dimensional systolic mechanics in canine ventricular myocardium. Am J Physiol 1999;276:H595–607.
82. Rademakers FE, Rogers WJ, Guier WH, et al. Relation of regional cross-fiber shortening to wall thickening in the intact heart. Three-dimensional strain analysis by NMR tagging. Circulation 1994;89: 1174–82.
83. Ingels NB Jr., Daughters GT 2nd, Stinson EB, Alderman EL. Measurement of midwall myocardial dynamics in intact man by radiography of surgically implanted markers. Circulation 1975;52: 859–67.
84. Beyar R, Yin FC, Hausknecht M, Weisfeldt ML, Kass DA. Dependence of left ventricular twist-radial shortening relations on cardiac cycle phase. Am J Physiol 1989;257:H1119–26.
85. Notomi Y, Setser RM, Shiota T, et al. Assessment of left ventricular torsional deformation by Doppler tissue imaging: validation study with tagged magnetic resonance imaging. Circulation 2005;111:1141–7.
86. Notomi Y, Lysyansky P, Setser RM, et al. Measurement of ventricular torsion by two-dimensional ultrasound speckle tracking imaging. J Am Coll Cardiol 2005;45:2034–41.
87. Gibbons Kroeker CA, Ter Keurs HE, Knudtson ML, Tyberg JV, Beyar R. An optical device to measure the dynamics of apex rotation of the left ventricle. Am J Physiol 1993;265:H1444–9.
88. Kroeker CA, Tyberg JV, Beyar R. Effects of ischemia on left ventricular apex rotation. An experimental study in anesthetized dogs. Circulation 1995;92:3539–48.
89. Ingels NB Jr., Hansen DE, Daughters GT 2nd, Stinson EB, Alderman EL, Miller DC. Relation between longitudinal, circumferential, and oblique shortening and torsional deformation in the left ventricle of the transplanted human heart. Circ Res 1989;64:915–27.
90. Rademakers FE, Buchalter MB, Rogers WJ, et al. Dissociation between left ventricular untwisting and filling. Accentuation by catecholamines. Circulation 1992;85:1572–81.
91. Taber LA, Yang M, Podszus WW. Mechanics of ventricular torsion. J Biomech 1996;29:745–52.
92. Kilner PJ, Yang GZ, Wilkes AJ, Mohiaddin RH, Firmin DN, Yacoub MH. Asymmetric redirection of flow through the heart. Nature 2000;404:759–61.
93. Cooke J, Hertzberg J, Boardman M, Shandas R. Characterizing vortex ring behavior during ventricular filling with Doppler echocardiography: an in vitro study. Ann Biomed Eng 2004;32:245–56.
94. Voon WC, Su HM, Yen HW, et al. Isovolumic relaxation flow propagation velocity in patients with diseases impairing ventricular relaxation. J Am Soc Echocardiogr 2005;18:221–5.
95. Gharib M, Rambod E, Kheradvar A, Sahn DJ, Dabiri JO. Optimal vortex formation as an index of cardiac health. Proc Natl Acad Sci U S A 2006;103:6305–8.
96. Buckberg GD. Tenth RESTORE Group Meeting: overview. Eur J Cardiothorac Surg 2006;29 Suppl 1:S213–5.
97. Hunter P, Nielsen P. A strategy for integrative computational physiology. Physiology (Bethesda) 2005;20:316–25.
98. Eschenhagen T, Zimmermann WH. Engineering myocardial tissue. Circ Res 2005;97:1220–31.

APPENDIX

To view videos and supplementary figures, please see the online version of this article.